Characterization of a novel temperate phage facilitating *in vitro* dispersal of multicellular bacteria

Hoda Jaffal[a], Mounia Kortebi[a], Pauline Misson[b*], Paulo Tavares[a], Malika Ouldali[a], Hervé Leh[a], Sylvie Lautru[a], Virginia S. Lioy[a], François Lecointe[b], Stéphanie Bury-Moné[a#]

[a]Université Paris-Saclay, CEA, CNRS, Institute for Integrative Biology of the Cell (I2BC), 91198, Gif-sur-Yvette, France

[b]Université Paris-Saclay, INRAE, AgroParisTech, Micalis Institute, Jouy-en-Josas, France

[#]Address correspondence to Stéphanie Bury-Moné, stephanie.bury-mone@i2bc.paris-saclay.fr

[*]Present addresses: Medical Research Council London Institute of Medical Sciences, London, United Kingdom; Institute of Clinical Sciences, Faculty of Medicine, Imperial College London, London, United Kingdom

Running title: Phage-mediated dispersal of multicellular bacteria

Word count for the abstract: 117

Word count for the text: 5051 (excluding titles and subtitles)

ABSTRACT

Streptomyces are renowned for their prolific production of specialized metabolites with applications in medicine and agriculture. These multicellular bacteria present a sophisticated developmental cycle, and play a key role in soil ecology. Little is known about *Streptomyces*-phage interactions and the impact of phages on *Streptomyces* physiology. In this study, we investigated the conditions governing the expression and production of 'Samy', a prophage found in *Streptomyces ambofaciens* ATCC 23877. This siphoprophage is produced simultaneously with the activation of other mobile genetic elements. We show that Samy production increases bacterial dispersal under *in vitro* stress conditions. Altogether, we unveiled a new property of a bacteriophage infection that it is closely linked to the multicellular community life of *Streptomyces* bacteria.

IMPORTANCE

Streptomyces are multicellular bacteria producing valuable metabolites, including antibiotics, with applications in medicine and agriculture. In this study, we characterized a novel temperate phage, named Samy, and its impact on bacteria physiology. Remarkably, the presence and production of Samy increases bacterial dispersal under *in vitro* stress conditions. This constitutes an emerging property associated with bacteriophage infection that might enhance the spread of the species. Our study reveals a new aspect of bacteriophage infection in the context of multicellular aggregate dynamics.

MAIN TEXT

INTRODUCTION

Streptomyces are among the most prolific producers of specialized metabolites, with applications in medicine and agriculture (1, 2). These filamentous Gram-positive bacteria are widely distributed in the environment and play a key role in soil ecology (3, 4). *Streptomyces* are a rare example of multicellular bacteria capable of forming hyphae with connected compartments. They present a complex life cycle that involves uni- to multi-cellular transitions, sporulation, metabolic differentiation, programmed cell death and exploration (3, 5).

While *Streptomyces* is the largest prokaryotic genus with over 900 species (Genome Taxonomy Database, Release 08-RS214), relatively few *Streptomyces* phages have been characterized to date. They represent less than 2.5% of the bacterial viruses listed by the ICTV (Release 21-221122_MSL37) or the NCBI, and only 7.5 % of the Actinobacteriophage Database (6). The identified *Streptomyces* phages are double stranded DNA viruses (Caudovirales and *Tectiviridae*), with the possible exception of an RNA virus detected in a *Streptomyces* transcriptome (7). Nevertheless, research on phage diversity and impact on *Streptomyces* physiology and ecology is still in its infancy, with only a few examples to date (8).

By causing lysis of their host, some *Streptomyces* phages are likely to contribute to the death process of a part of the colony and/or to premature termination of antibiotic production. Accordingly, they can lead to industrial fermentation failure (9). Moreover, *Streptomyces* - phage interplay may also encompass specific traits linked the complex life cycle of these bacteria. For instance, some phages can induce the release of specialized metabolites (10, 11). Reciprocally, some bioactive compounds produced by *Streptomyces* can act as anti-phage defenses (12–14). Furthermore, some *Streptomyces* phages encode

homologs of sporulation and antibiotic production regulators (15), and can impact the developmental cycle of *Streptomyces* (11). Reciprocally, susceptibility to phage infection varies along this cycle (11, 16).

The last few years have been marked by a sustained effort in the isolation and sequencing of *Streptomyces* phages from environmental samples (17–19, 10, 20, 21). Moreover, the *Streptomyces* genome can constitute *per se* a viral genetic reservoir, through the genomes of temperate prophages that they may host. Using PHASTER (22), prophage sequences were detected in all *Streptomyces* strains that were analyzed (*n* = 7) (23). The prophage state is, perhaps, one of the most important stages in the interaction between phage and host genomes. Indeed, the lysogenic cycle represents an opportunity for phages to confer new properties to their host notably through the expression of moron genes that may contribute to bacterial fitness and environmental niche expansion (24).

In this study, we characterize a novel temperate phage from *Streptomyces ambofaciens* ATCC 23877, which we named 'Samy'. This phage is produced under metabolic stress and activated at the same time as other mobile genetic elements. We observed that this production promotes bacterial dispersal under *in vitro* stress conditions. This study reports a new property resulting from phage-bacteria interaction in the context of multicellularity.

MATERIALS AND METHODS

Streptomyces strains

The *Streptomyces* strains and primers used in this study are listed in **Table S1** and **Table S2**, respectively. A CRISPR-Cas9-based approach using a single guide RNA (SBM395, **Table S2**) targeting the Samy integrase (SAMYPH_94/ SAM23877_RS39280) was conducted in the absence of a template donor DNA using pCRISPR-Cas9 vector, as previously described (25). The precise size of the deleted regions in 3 independent clones was determined by sequencing (**Table S1, Figure S1**).

Growth conditions

All media composition are described in **Table S3**. Bacteria were grown at 30°C. Spores were collected after growth on SFM medium. About 10^7 spores were inoculated in 50 mL of liquid medium (in a 500 mL Duran® Erlenmeyer baffled flask with a silicon stopper) and incubated in a shaking orbital agitator (200 rpm, INFORS Unitron standard). Aliquots from

the cultures were collected, centrifuged and filtered using Whatman PVDF Mini-UniPrep syringeless filters (0.2 µm). Antibacterial activity against *Micrococcus luteus* was determined as previously described (26). The colony forming units (CFU) after 4 days of growth in BM liquid medium were determined after serial dilutions in water, and plating of 100 µl of dilutions on SFM medium. To analyze the impact of conditioned supernatants on *S. ambofaciens* growth and survival, the WT strain or its isogenic mutant ΔSamy clone #3 were grown in BM medium during 24 h before supplementing the medium with filtered conditioned supernatants at ratios of 1:2 or 1:5 (supernatant: culture volume). Then, the bacteria were grown for an additional 3 days before counting.

Optical microscopy

After 4 days-growth in BM liquid medium, 10 µL of *Streptomyces* cultures were directly mounted on glass coverslips and analyzed using an Olympus BX63 microscope. Images were acquired with a 40x oil immersion objective.

Phage quantification by qPCR

Filtered supernatants were treated with 1U/100 µL TURBO DNAse (Invitrogen) for 1 h at 37°C, and then incubated for 20 min at 80°C. Amplification was carried out on 2 µL of these treated supernatants, in a final volume of 10 µL, using the LightCycler FastStart DNA Master HybProbe kit (Roche Diagnostics) supplemented with SYBR Green. Primers used to amplify Samy prophage and a host gene are indicated in **Table S2**. The qPCR efficiencies as well as the absolute number of amplified copies were determined using 10^2 to 10^6 copies of *S. ambofaciens* ATCC 23877 gDNA as standard.

Infection assay

After 4 days-growth in BM liquid medium, *S. ambofaciens* ATCC 23877 culture was centrifuged at 8,000 rpm (JA14 rotor, Beckman) for 15 min at 4°C to pellet intact bacteria and debris. The supernatant was then transferred to new centrifuge tubes and subjected to overnight centrifugation under the same condition. The pellet was resuspended and serially diluted in TBT buffer (100 mM Tris-HCl, pH 7.5; 100 mM NaCl; 10 mM $MgCl_2$). Approximatively 10^8 spores of target bacteria [*Streptomyces albidoflavus* J1074, *S. ambofaciens* ATCC 23877, *S. ambofaciens* DSM 40497, *S. coelicolor* A3(2), *Streptomyces noursei* ATCC 11455, *Streptomyces rimosus* ATCC 10970, *Streptomyces venezuelae* ATCC 10712, **Table S1**] were inoculated in 3 mL of SNA before pouring on SFM plates.

Five µL of serial dilutions of the phage preparation were spotted on the bacterial lawns. The plates were incubated for one week before imaging.

Samy prophage detection and annotation

Synteruptor program (http://bim.i2bc.paris-saclay.fr/synteruptor/, v1.1) was used to compare the sequences of *S. ambofaciens* ATCC 23877 and *S. ambofaciens* DSM 40697 (26, 27), with a minimal threshold of 20 CDSs to identify genomic islands. PHASTER (22) was used to predict the presence of a putative prophage in the *S. ambofaciens* chromosome. *In silico* translated Samy prophage CDSs predicted in *S. ambofaciens* ATCC 28377 chromosomal sequence [CP012382, initial annotation (28)] were functionally annotated using HHPred (29) against the PDB mmCIF70 (version of January 10, 2023) and PHROGs_V4 (30) databases. Functions (known or unknown) of the nearest homologs were transferred to the queries by only retaining predictions with a probability ≥ 95.8%. The genome comparison between Samy and PhiC31 was performed using Easyfig software (e-value $<10^{-3}$, v2.2.5). No significant similarity with a previously annotated CDS led to a 'hypothetical protein' annotation. In case of identification of a protein related to an annotated PHROG of unknown function, the annotation of the gene is 'protein of unknown function' with a note indicating the related-PHROG number. This first annotation was manually curated using the more recently submitted version of *S. ambofaciens* ATCC 28377 chromosome annotation (NZ_CP012382, released 2022-04-14). The annotated genes have an identifier starting with "SAMYPH".

RNA preparation, sequencing and data processing

About 2.10^6 spores (in 5 µL) of *S. ambofaciens* ATCC23877 were spotted on a sterile cellophane covering the medium in the Petri dish. Thirty hours later, cells were harvested using a sterile cone and deposited into a tube containing 5 mL of cold ethanol. Cells were then harvested by centrifugation for 15 min at 4,000 *g* at 4°C, and stored at -20°C.

RNA extraction, sequencing and analysis was performed as previously described (26). The reads were mapped in terms of "Gene" and pseudogene features according to *S. ambofaciens* ATCC23877 annotation (GCF_001267885.1_ASM126788v1_genomic.gff – released 2022-04-14) and modified to include our own manual curation of Samy prophage annotation. The reference condition used to run the SARTools DESeq2-based R pipeline (31) was 24 h-growth in MP5 medium. Data were analyzed with R software (32). Gene ontology analysis g:Profiler:g:GOSt software (https://biit.cs.ut.ee/gprofiler/gost, version

e109_eg56_p17_1d3191d) was performed as previously described (23). The 'mclust' R package (33) was used to identify the gene populations of Samy prophage transcriptomes, via a Gaussian finite mixture model fitted by the expectation-maximization algorithm.

Virion purification by CsCl gradient

About 2.10^6 spores of *S. ambofaciens* ATCC 23877 were inoculated in 2 L of BM medium. After 4 days-growth, the culture was centrifuged at 8,000 rpm (JA14 rotor, Beckman) for 15 min at 4°C to pellet intact bacteria and debris. The supernatant was then transferred to new centrifuge tubes and subjected to overnight centrifugation under the same condition. The pellet was resuspended in 18 mL of TBT buffer and treated with 2 U/mL TURBO DNAse (Invitrogen) and 100 µg/mL RNAse for 1 h at 37°C. The phage was purified by isopycnic centrifugation in a CsCl discontinuous gradient for 5 h at 32,000 rpm in a SW41 rotor (Beckman) at 20°C, as previously described (34).

Transmission electron microscopy (TEM)

Phage samples collected after 4 days-growth in 1 L of HT liquid medium were concentrated for TEM observation by successive washes in ammonium acetate as previously described (35). To eliminate debris and/or dextrin, a second set of TEM observations using the negative staining method was conducted on CsCl-purified particles produced in BM medium. Three µl of sample suspension were deposited on an air glow-discharged 400 mesh copper carbon-coated grid for 1 min. Excess liquid was blotted, and the grid rinsed with 2 % w/v aqueous uranyl acetate. The grids were visualized at 100 kV with a Tecnai 12 Spirit TEM microscope (Thermo Fisher, New York NY, USA) equipped with a K2 Base 4k x 4k camera (Gatan, Pleasanton CA, USA).

Virome sequencing and data processing

DNA from CsCl-purified particles was extracted twice with phenol, once with chloroform, and dialyzed overnight against 10 mM Tris–HCl (pH 7.5) and 0.1 mM EDTA. After random fragmentation, the DNA sample was paired-end sequenced using Illumina dye sequencing as previously described (36). Data were analyzed with the Integrative Genomics Viewer (IGV) tool (37). STAR software (38) and *featureCounts* program (39) were used to quantify total reads along the reference genome containing only one terminal inverted repeat (TIR). The sequence coverage at termini position was identified using PhageTerm (Version 1.0.12) (40).

RESULTS

Identification of Samy, a complete prophage, in the *S. ambofaciens* ATCC 23877 chromosome

The comparison of *S. ambofaciens* ATCC 23877 genome to the closely related strain DSM 40697 led to the identification of a genomic island (≈ 71 kb, 113 genes - **Fig. 1A**), which is remarkably large. Indeed only 12% of *S. ambofaciens* ATCC 23877 genomic islands exceed 45 genes (26). This region exhibits the lowest GC content (66.0%) and is predicted to contain a complete prophage by PHASTER (**Fig. 1A**). This latter, further named 'Samy', is exclusively present in the ATCC 23877 strain, and stands as the sole complete prophage identified in its genome. The ATCC 23877 and DSM 40697 strains share 99.04 % of average nucleotide identity calculated by using the BLASTn algorithm (ANIb) (23), indicating that they belong to the same species. The absence of Samy in the DSM 40697 strain indicates that the infection is relatively recent, *i.e.* occurred after speciation. The identification of a direct repeat ('TCGGGTGTGTCG') in front of a serine integrase gene and approximately 61 kb downstream prompted us to propose this sequence as belonging to the left (*attL*) and right (*attR*) attachment sites of the Samy prophage (6,589,778-6,650,857 bp position in the *S. ambofaciens* ATCC 23877 chromosome). Immediately upstream, a region of approximately 10 kb contains only a few phage genes, including one coding for a putative integrase, indicating that it may correspond to a remnant prophage (**Fig. 1B**). The mosaic composition of the genomic island suggests that it is located in a region prone to integration and/or fixation of exogenous sequences.

Samy prophage presents a typical GC content (66.53 %) and size (61.07 kb, 102 genes) compared to other *Streptomyces phages* (**Fig. S2, Table S4**). Annotation of Samy sequence allowed identification of most structural genes that are essential to form a complete phage (*e.g.* encoding head, neck and tail proteins, base plate and tail fiber proteins) as well as replication proteins, endolysin, several nucleases, transcriptional regulators, integrase and recombination directionality factor (**Fig. 1.C**, **Table S5**). Altogether, these analyses suggested that this prophage may be able to produce viral particles. This led us to investigate the conditions for its expression.

Activation of Samy prophage and other mobile genetic element expression is correlated with a general stress response

The linear chromosome of *S. ambofaciens* ATCC23877 is delimited by distal ribosomal RNA (*rrn*) operons into distinct spatial compartments (23, 26). The terminal compartments are enriched in poorly conserved sequences and exhibit lower transcriptional activity compared to the rest of the chromosome (23, 26). The expression of these variable regions is generally conditional *i.e.* induced under specific conditions such as the stationary growth phase in MP5 medium for the cluster encoding congocidine antibiotic biosynthesis (41). An empirical approach is often required to characterize the inducing conditions such as the OSMAC ("One Strain Many Compounds") approach, based on strain cultivation in different environmental conditions (42). We used a similar approach by analyzing the Samy transcriptome in 13 growth conditions including routine *Streptomyces* complex or minimal media (**Table S5**), liquid or solid conditions, and different time points (**Fig. 2**, **Fig. S3**). We observed three conditions of 30 h growth on plates (named 'HT', 'ONA' or 'NAG') in which Samy prophage is globally expressed, suggesting that the lytic cycle of Samy was induced. Its expression level was the strongest in 'HT' condition (**Fig. 2.A**). HT medium was developed by Hickey and Tresner (43) to induce sporulation of *Streptomyces* strains that sporulate poorly on growth media classically used for this purpose. Interestingly, HT condition is also associated with strong expression of several sequences from mobile genetic elements: the pSAM1 plasmid (**Fig. 2.B, Fig. S4.A**), the integrative conjugative element (ICE) pSAM2 (**Fig. 1.A** & **2.B, Fig. S4.B**) as well as several other genes of phage origin such as two orthologs of phage tail-like nanostructures previously identified as extracellular contractile injection systems (eCIS) (44, 45) (SAM23877_RS16255, SAM23877_RS16260), and two genes outside a proviral context (the phage tail protein SAM23877_RS23520, and the phage holin family protein SAM23877_RS09270). We confirmed that Samy phage was produced in HT liquid medium (≈ 10^6 phages/ml) but not MP5 medium by performing qPCR (**Fig. 3**).

We analyzed Samy transcriptomes in non or poorly inducing conditions (> 38 % of Samy genes remaining in the lowest 'CAT_0' category *i.e.* all conditions except 'HT', 'ONA', 'NAG'). In these conditions, the Samy transcriptome presents a bimodal pattern, as previously described for other phages (35) (**Fig. S5**). The most transcribed genes in non or poorly inducing conditions could be involved in the lysogenic cycle of Samy or could be

morons, *i.e.* genes involved in the fitness of the bacteria under these growth conditions or in their resistance to other phages (**Fig. 2.A, Table S6**). Among them, the gene we annotated as a putative immunity repressor (SAMYPH_32/SAM23877_6125) was highly expressed under all conditions tested, reinforcing our prediction.

We determined host transcriptome characteristics during Samy awakening by comparing the three conditions associated with Samy induction ('HT', 'ONA', 'NAG') to the closest control condition, lacking Samy induction (**Fig. S3.B & C**). This latter corresponds to 30 h growth on mannitol minimal medium plate ('MM' condition). GO enrichment and DESeq2 analyses revealed that Samy is induced in conditions associated with a strong repression of genes related to nitrogen assimilation (**Table S5**). Several genes linked to adaptation to osmotic and oxidative stresses are also co-up-regulated with Samy. They notably encode gas vesicles, ectoine and ergothioneine biosynthesis processes (**Table S5**). Moreover, several sigma factors are differentially expressed in the 'HT' condition (compared to the 'MM' condition): six are induced including SigE, a regulator of cell envelope integrity (46) and SigF which is required for sporulation (47). Ten sigma factors are repressed including the principal sigma factor SigA (**Table S5**). Altogether, these data indicate that the 'HT' condition is associated with a profound transcriptional change, probably reflecting a stressful situation.

In parallel, the genes in the GO functional categories 'translation' and 'arginine biosynthetic process' were strongly repressed (adjusted *p* values, calculated by g.Profiler, of 3.7×10^{-6} and 5.6×10^{-6}, respectively). Indeed, 34 host tRNAs were repressed whereas all 4 of Samy's tRNAs were induced. This illustrates how tRNA expression can be part of phage strategy in a translation inhibiting situation.

The SOS response is classically associated with the activation of prophages, and has recently been described in *S. venezuelae* (48). In *S. ambofaciens* ATCC 23877, transcripts of the key actors of the SOS response such as RecA, LexA, RecN, DnaE, RuvA Holliday junction DNA helicase (48) were not up-regulated in the 'HT' condition compared to the 'MM' reference (**Table S5**). This result suggests that the SOS response is not involved in the induction of Samy production in the 'HT' condition, or may be so transient and/or only present in part of the cell population that it was not detected by our bulk transcriptome analysis. Moreover, addition of mitomycin C DNA crosslinker and ciprofloxacin topoisomerase poison in MP5 medium, at the minimal concentrations that inhibit bacterial growth (1 and 2 µg/mL, respectively), did not induce Samy production measured by qPCR at 30 min, 2 h and 24 h (Ct > 28, 3 independent experiments). This observation reinforces

the hypothesis that the SOS response may not be involved in the induction of Samy, at least under our study conditions.

To conclude, in our study the activation of Samy and other genetic elements is correlated with huge physiological changes associated notably with nitrogen imbalance and translation inhibition and a general stress response.

Samy production increases in alkaline conditions

In order to determine the key compounds responsible for Samy induction, and to set up monitoring of its production in liquid medium, we tested variants of the HT liquid medium by eliminating one or more of its constituents. The simplest version of a medium associated with high viral titers, as quantified by qPCR, was named "BM" (for “Bacteriophage production Medium”) (**Fig. 3**). We noted a fairly high inter-experimental variability in Samy titer in BM medium (8.10^6 up to 2.10^{10} phage/ml depending on the experiment), which might reflect its stochastic induction within the cell population. However, production kinetics is the same in all experiments: Samy particles are released between 24 and 48h of growth in BM medium, the titer being almost constant over the following days (**Fig. 4.A**).

Interestingly, we observed a positive correlation between viral titer and pH which is statistically significant (Spearman's rank correlation rho = 0.73, *p* value = 0.016). Indeed, adding buffering compounds (*e.g.* MOPS or dextrin) in BM medium strongly decreased phage production (**Fig. 3**). These results indicate that alkalinity constitutes an additional signal triggering Samy production and/or increasing virion stability in the supernatant.

Samy is a new active siphophage

TEM revealed that Samy is a siphophage with a capsid diameter of 65.4 $\pm$ 2.8 nm (*n* = 35), and a long rather rigid tail 248.7 $\pm$ 7.4 nm in length (*n* = 32) and 11.7 $\pm$ 0.4 nm thick (*n*=12) (**Fig. 4B**, **Fig. S6.A-B**). Remarkably, Samy virions are co-purified with eCIS (**Fig. S6. A-B**) consistently, with the transcription of the orthologous genes encoding this system (SAM23877_RS16255, SAM23877_RS16260) in the ‘HT’ condition (**Table S5**).

High-throughput sequencing of these CsCl-purified particles revealed that Samy phage is the only double stranded DNA phage produced in this condition. In total, 8,671,900 (99.5%) out of 8,712,953 reads successfully aligned to the *S. ambofaciens* ATCC 23877 genome corresponded to Samy. The remaining reads mapped all along the *S. ambofaciens* genome and may correspond to contaminating bacterial DNA and/or transduced DNA. The analysis of sequence coverage at termini positions allowed the

prediction of the Samy cohesive *cos* sequence ('CGTTAAGGTGC', **Fig. S7**). Reads confirmed the borders of the prophage and did not show any trace of lateral transduction, consistent with a *cos* packaging mechanism (**Fig. S7**).

Finally, Samy virions are infectious since we observed plaques using *Streptomyces lividans* TK24 strain as a host (**Fig. S6.C**). Strikingly, no lysis plaque could be obtained during the infection assays conducted on 7 other strains listed in **Table S1**, including two S. *ambofaciens* strains. The absence of superinfection of strain ATCC 23877 is expected, since prophage-bearing strains generally express an immunity repressor. For the other strains, these results indicate that Samy infection has a fairly narrow spectrum and/or requires lab conditions that were not reproduced in these experiments.

Altogether, these results indicate that Samy is an active prophage that encodes a complete and infectious siphophage.

Impact of Samy phage on *Streptomyces* growth and antibiotic production

We first compared ATCC 23877 (Samy^{+}) and DSM 40697 (Samy^{-}) strain growth in BM medium, using MP5 medium as a control. Surprisingly, the exponential phase of growth started about 8 h earlier in BM than in MP5 medium, suggesting that germination was more efficient or rapid in this condition (**Fig. 5.A**). At later stages of growth, the increase in biomass stopped in BM medium quite early (at a pseudo-opacimetry of about 1) whereas it reached higher densities in MP5 medium (**Fig. 5.A**). We found that this cessation of growth in BM medium correlated with the alkalinity of the medium (**Fig. 5.A**). In addition, both strains presented different phenotypes in the following days of growth in BM medium: while the strain ATCC 23877 remained relatively dispersed at a density that did not drop much, strain DSM 40697 formed large pellets (**Fig. 5.B**).

We used a CRIPSR approach to obtain ATCC 23877 derivate deleted for part or all of the prophage (**Table S1**). Although the three clones tested carry different Samy deletions, they all presented the same phenotype. After 4 days of growth, aggregates appeared in the cultures, but not in the parental strain (**Fig. 5.B**). Microscopic observations of the cultures confirmed the formation of larger and denser cell pellets in the absence of the prophage (**Fig. 5.C, Fig. S8.A**). Interestingly, the formation of cell aggregates during growth in BM medium was also observed with *S. coelicolor* A(3)2, another *Streptomyces* species that do not contain Samy or any other PHASTER predicted complete prophage (**Fig. S8.B**). The DSM 40697 strain however exhibits larger aggregates in BM medium

compared to the ATCC strain devoid of the complete Samy prophage, suggesting that prophage induction is only one of the factors influencing cluster size under these specific conditions.

Because of the multicellular nature of *Streptomyces*, the CFU count not only reflects cell survival, but also the number of multicellular clusters *per se* regardless of the number and proportion of living or dying cells in the clusters. Thus, we hypothesized that Samy induction could modify the number of culturable and viable colonies in the medium. We determined the number of CFUs after 4 days growth in BM medium of the strains ATCC 23877 (Samy$^+$), DSM 40697 (Samy$^-$) and ATCC 23877 Δ*Samy*. To optimize bacterial growth after stressing conditions, counting were carried out on Soy Flour Mannitol (SFM) medium, widely used for routine cultivation of *Streptomyces* species since it promotes the sporulation of most of them (49). Remarkably, the number of CFUs was around 2-logs higher in the phage-producing ATCC 23877 strain than in its phage-deleted derivative or the DSM 40697 strain (**Fig. 5.D**). Thus, the activation of Samy prophage was correlated with a drastic increase in the number of viable multicellular clusters formed by the ATCC 23877 parental strain. During a return to a condition more favorable to growth (exemplified here by the SFM medium used to count the colonies), this property resulted in an increase in the number of CFUs compared to strains having formed larger cell aggregates.

To evaluate the potential impact of storage and strain evolution in laboratory conditions on the growth phenotype, we performed a comprehensive analysis on multiple *S. ambofaciens* strains (harboring or not Samy prophage) sourced from diverse collections (**Table S1**). Once again, we observed a positive correlation ($R = 0.75$, $p = 0.00074$, Spearman method) between the production of Samy and the number of CFUs following a four-day growth period in BM medium (**Fig. 5.E**).

In order to test whether a soluble factor present in the culture supernatant could contribute to the dispersal phenotype, we added a conditioned supernatant of the parental strain grown 4 days in BM medium to a 24 h culture of the phage-deleted strain. We found no increase in colony number after 4 days of incubation in BM medium (**Fig. S9**), indicating that the prophage needs to be present within the cells to increase the *in vitro* dispersal.

Finally, we evaluated the impact of Samy phage production on antibacterial activity, a key step in the development cycle of *Streptomyces*. Interestingly, the antibacterial activity of the ATCC 23877 strain in BM condition is not affected by the presence or absence of an intact prophage copy (**Fig. 5.F**).

Altogether these results indicate that the induction and production of Samy prevents the formation of large cell aggregates by *S. ambofaciens* ATCC 23877 in a stressful condition, promoting bacterial dispersal *in vitro*, without causing a massive death of antibiotic-producing cells.

DISCUSSION

In this study we describe the conditions of awakening of a *Streptomyces* prophage associated with profound physiological changes within the colony. In HT broth, a medium initially optimized to promote *Streptomyces* sporulation (43), we have described for the first time a massive activation of mobile genetic element expression (Samy prophage, pSAM1 plasmid and pSAM2 ICE; **Fig. 2, Fig. S4**) and other phage-related genes such as those encoding eCIS (44, 45) (**Fig. S6.A** and **Table S5**), as well as a high stress situation associated with an imbalance in nitrogen metabolism and translation inhibition (**Table S5**).

This phenomenon seems to be concomitant with physiological modifications that may contribute to strain dispersal in this condition. For instance, we observed increased expression of the genes encoding the synthesis of geosmin and 2-methylisoborneol volatile compounds (**Table S5**) which may promote spore dispersal by animals (8, 50). Moreover, a hydrophobic layer of chaplins may also contribute to their dispersion by limiting their loss in the anoxic depths of the soil, and by mediating their adhesion to hydrophobic surfaces (51). The induction of the expression of genes encoding gaseous vesicles (**Table S5**) may also contribute to the flotation and propagation of *Streptomyces* (52). Phage production thus seems to be part of a more general stress and/or dispersal response.

Samy is most likely activated through an SOS-independent pathway, with the precise signal(s) for Samy prophage induction yet to be determined. ‘NAG’, ‘ONA’, ‘HT’ and ‘BM’ conditions do not share a common compound but are all associated with the induction of Samy expression. The N-acetyl-glucosamine present in the ‘NAG’ condition (but absent in the ‘MM’ medium) is required to induce Samy expression. This molecule is a monomer of chitin which acts as a signal molecule and activates development and antibiotic production under poor growth conditions (53). On the other side, ONA, HT and its BM derivate are characterized by the presence of beef meat (**Table S3**, **Fig. 3**). Moreover, alkalinity constitutes an additional stress signal correlated with the induction of Samy and/or enhancing phage particle stability (**Fig. 3**). Interestingly, alkaline conditions are also required for the initiation of the ‘explorer’ phenotype in *S. venezuelae* (54). Altogether these observations indicate that multiple factors can promote Samy induction.

Most of our experiments were conducted under liquid growth conditions, a situation actually similar to those of most industrial bioreactors. It has long been described that the appearance of *Streptomyces* growth in liquid media (dispersed hyphae *versus* pellets or clumps) depends on the state of the initial inoculum and varies from one species to another (55). “Fragmentation of the mycelial clumps” (56) or “pellet fragmentation” (57) in liquid medium have even been reported for some species. The biophysical parameters that may influence the type of hyphae grouping in liquid medium have been explored for a few strains (42). Some genetic factors such *ssgA* morphogene (56) also contribute to the morphology of *Streptomyces* mycelia in submerged cultures. Mycelium fragmentation may actually be a key contributor to strain spread in liquid medium, since most *Streptomyces,* like *S. ambofaciens* ATCC 23877, sporulate poorly or not at all during submerged growth. In this study, we demonstrate for the first time that a prophage can contribute to a similar process by promoting the formation of small and numerous clumps favoring strain dispersal, and increasing by 2-logs the number of clumps/pellets able to give rise to new colonies. Samy belongs to the group of Caudovirales which are released by cell lysis. So we propose that cell death induced by Samy in part of the colony contributes to this strain dispersal (**Fig. 6**). The fact that partial deletion of Samy (in the integrase coding region) is sufficient to abolish the phenotype, supports the view that viral production is required.

Samy phage production takes place mainly between 24 h and 48 h of growth in BM medium (**Fig. 4.A**), leading to a final phage titer that is quite variable from one experiment to another (**Fig. 3**). This suggests that the triggering of phage production in the population may be stochastic. Only a portion of the cells die as evidenced by the lack of impact on overall antibiotic production in BM liquid medium (**Fig. 5.F**), the high number of CFU after 4 days-growth in this medium (**Fig. 5.D**) and the effective sporulation of the strain on solid HT medium (our personal observations). The fact that the putative immune repressor is still expressed in ‘HT’ conditions reinforces these observations as this is characteristic of transcriptomes made on heterogeneous populations with respect to phage production, as previously reported (35). Thus, we favor a model in which only a fraction of the cells will die, allowing the preservation of the remainder of the colony or cell aggregate. Assuming that Samy-mediated dispersion may provide a selective advantage under certain conditions (*e.g.* switch from BM to SFM growth condition), its production could illustrate a division of labor leading to an 'altruistic' loss of fitness within a subpopulation of cells (59).

The similarities between *Streptomyces* mycelium fragmentation and biofilm dispersal have been previously highlighted (57). Moreover, the use of phages is presented as a

promising approach to control biofilms (60). Our study highlights the possible risk of bacterial dispersal that may be associated with the (partial) induction of prophages in cellular aggregates. Phage-mediated dispersal of biofilms has also been reported in *Enterococcus faecalis* unicellular bacteria (61). Another prophage, in *Pseudomonas aeruginosa*, has already been shown to have an impact on bacterial biofilms by consolidating them through the contribution of extracellular DNA (62). Our study further emphasizes the importance of considering prophages into models exploring multicellular aggregate dynamics and/or transitions to multicellular life (63).

Data Availability

The RNA-seq data generated during this study have been deposited in the NCBI Gene Expression Omnibus (GEO, https://www.ncbi.nlm.nih.gov/geo/) under the accession code **GSE232795** (https://www-ncbi-nlm-nih-gov.insb.bib.cnrs.fr/geo/query/acc.cgi?acc=GSE232795). The virome sequencing data are available in the bioproject PRJNA974565 on **SRA** (https://www.ncbi.nlm.nih.gov/bioproject/974565). We used RNA-seq data available under the accession code **GSE162865** (https://www-ncbi-nlm-nih-gov.insb.bib.cnrs.fr/geo/query/acc.cgi?acc=GSE162865) (26). Samy phage complete sequence is available on GenBank under the following accession number: OR263580.1. The Bioproject accession number of this study is PRJEB62744.

APPENDIXES

Supplementary Fig. S1: Schematic representation of deletions generated by a CRIPSR-Cas9 approach targeting Samy prophage integrase

Supplementary Fig. S2: GC content (A) and size (B) of a panel of 330 *Streptomyces* phages

Supplementary Fig. S3: Multidimensional analyses of the transcriptomes of *S. ambofaciens* ATCC 23877 grown under various conditions

Supplementary Fig. S4: Heatmaps of pSAM1 (A) and pSAM2 (B) transcriptomes in different growth conditions

Supplementary Fig. S5: Samy expression profile under the different conditions studied

Supplementary Fig. S6: Samy phage morphology and infection assays

Supplementary Fig. S7: Results of high-throughput sequencing of the double-stranded DNA virome of *Streptomyces ambofaciens* ATCC 23877 grown 4 days in BM medium

Supplementary Fig. S8: Morphology of *S. ambofaciens* and *S. coelicolor* after 4 days growth in BM medium

Supplementary Fig. S9: Counting of colony forming units after 4 days of growth in BM medium of *S. ambofaciens* ATCC 23877 reference strain and its isogenic ΔSamy #clone 3 mutant supplemented with conditioned supernatants

Table S1: Strains used in this study

Table S2: Primers used in this study

Table S3: Media used in this study

Table S4: List and characteristics of 330 *Streptomyces* phages referenced in Actinophage Database, NCBI and/or ICTV. The legend is detailed in the “Readme” sheet.

Table S5: Results from the OSMAC-RNAseq approach conducted in *Streptomyces ambofaciens* ATCC 23877. The legend is detailed in the “Readme” sheet.

Table S6: List of Samy genes overexpressed in non or poorly inducing conditions. The legend is detailed in the “Readme” sheet.

ACKNOWLEDGMENTS

This work was supported by the *Agence Nationale pour la Recherche* [ANR-21-CE12-0044-01/STREPTOMICS]. We thank Jean-Luc Pernodet and Frederic Boccard for their precious

support. We also would like to thank Christine Longin (MIMA2 platform) for her help with TEM observations and Julien Lossouarn for his help in annotating phage genes and submitting Samy's genome. We thank Soumaya Najah and Corinne Saulnier for their technical help. We are grateful to Vinciane Regnier and Logan Greibill for valuable training on the Olympus BX63 microscope. We also thank Pascaline Tirand for her daily help.

CONFLICT OF INTEREST

The authors declare no competing interests.

REFERENCES

1. Berdy J. 2012. Thoughts and facts about antibiotics: where we are now and where we are heading. J Antibiot (Tokyo) 65:385–95.

2. Donald L, Pipite A, Subramani R, Owen J, Keyzers RA, Taufa T. 2022. Streptomyces: Still the Biggest Producer of New Natural Secondary Metabolites, a Current Perspective. Microbiology Research 13:418–465.

3. Barka EA, Vatsa P, Sanchez L, Gaveau-Vaillant N, Jacquard C, Meier-Kolthoff JP, Klenk HP, Clement C, Ouhdouch Y, van Wezel GP. 2016. Taxonomy, Physiology, and Natural Products of Actinobacteria. Microbiol Mol Biol Rev 80:1–43.

4. Prudence SMM, Addington E, Castaño-Espriu L, Mark DR, Pintor-Escobar L, Russell AH, McLean TC. 2020. Advances in actinomycete research: an ActinoBase review of 2019. Microbiology 166:683–694.

5. Jones SE, Elliot MA. 2017. Streptomyces Exploration: Competition, Volatile Communication and New Bacterial Behaviours. Trends in Microbiology 25:522–531.

6. Russell DA, Hatfull GF. 2017. PhagesDB: the actinobacteriophage database. Bioinformatics 33:784–786.

564 7. Krishnamurthy SR, Janowski AB, Zhao G, Barouch D, Wang D. 2016. Hyperexpansion of RNA
565 Bacteriophage Diversity. PLoS Biol 14:e1002409.

566 8. Shepherdson EM, Baglio CR, Elliot MA. 2023. Streptomyces behavior and competition in the
567 natural environment. Current Opinion in Microbiology 71:102257.

568 9. Lu N, Kim C, Chen Z, Wen Y, Wei Q, Qiu Y, Wang S, Song Y. 2019. Characterization and genome
569 analysis of the temperate bacteriophage φSAJS1 from Streptomyces avermitilis. Virus Research
570 265:34–42.

571 10. Hardy A, Sharma V, Kever L, Frunzke J. 2020. Genome Sequence and Characterization of Five
572 Bacteriophages Infecting Streptomyces coelicolor and Streptomyces venezuelae: Alderaan,
573 Coruscant, Dagobah, Endor1 and Endor2. Viruses 12:1065.

574 11. Luthe T, Kever L, Hänsch S, Hardy A, Tschowri N, Weidtkamp-Peters S, Frunzke J. 2023.
575 *Streptomyces* development is involved in the efficient containment of viral infections. microLife
576 4:uqad002.

577 12. Kronheim S, Daniel-Ivad M, Duan Z, Hwang S, Wong AI, Mantel I, Nodwell JR, Maxwell KL. 2018. A
578 chemical defence against phage infection. Nature 564:283–286.

579 13. Kever L, Hardy A, Luthe T, Hünnefeld M, Gätgens C, Milke L, Wiechert J, Wittmann J, Moraru C,
580 Marienhagen J, Frunzke J. 2022. Aminoglycoside Antibiotics Inhibit Phage Infection by Blocking an
581 Early Step of the Infection Cycle. mBio 13:e00783-22.

582 14. Hardy A, Kever L, Frunzke J. 2023. Antiphage small molecules produced by bacteria – beyond
583 protein-mediated defenses. Trends in Microbiology 31:92–106.

584 15. Sharma V, Hardy A, Luthe T, Frunzke J. 2021. Phylogenetic Distribution of WhiB- and Lsr2-Type
585 Regulators in Actinobacteriophage Genomes. Microbiol Spectr 9:e00727-21.

586 16. Rosner A, Gutstein R. 1981. Adsorption of actinophage Pal 6 to developing mycelium of
587 *Streptomyces albus*. Can J Microbiol 27:254–257.

588 17. Jordan TC, Burnett SH, Carson S, Caruso SM, Clase K, DeJong RJ, Dennehy JJ, Denver DR, Dunbar D,
589 Elgin SCR, Findley AM, Gissendanner CR, Golebiewska UP, Guild N, Hartzog GA, Grillo WH,
590 Hollowell GP, Hughes LE, Johnson A, King RA, Lewis LO, Li W, Rosenzweig F, Rubin MR, Saha MS,
591 Sandoz J, Shaffer CD, Taylor B, Temple L, Vazquez E, Ware VC, Barker LP, Bradley KW, Jacobs-Sera
592 D, Pope WH, Russell DA, Cresawn SG, Lopatto D, Bailey CP, Hatfull GF. 2014. A Broadly
593 Implementable Research Course in Phage Discovery and Genomics for First-Year Undergraduate
594 Students. mBio 5:e01051-13.

595 18. Fogg PCM, Haley JA, Stark WM, Smith MCM. 2017. Genome Integration and Excision by a New
596 Streptomyces Bacteriophage, Joe. Appl Environ Microbiol 83:e02767-16.

597 19. Sharaf A, Mercati F, Elmaghraby I, Elbaz RM, Marei EM. 2017. Functional and comparative genome
598 analysis of novel virulent actinophages belonging to Streptomyces flavovirens. BMC Microbiol
599 17:51.

600 20. Ongenae V, Azeredo J, Kropinski AM, Rozen D, Briegel A, Claessen D. 2022. Genome sequence and
601 characterization of Streptomyces phage Pablito, representing a new species within the genus
602 Janusvirus. Sci Rep 12:17785.

603 21. Park YG, McCarthy GF, Mustafa H, Feild GM, Puram S, Younes HA, Imam D, 2021 UMBC Phage
604 Hunters, STEM BUILD at UMBC Cohort 5, Erill I, Caruso SM. 2022. Complete Genome Sequences of
605 *Streptomyces* Bacteriophages Annihilus, TonyStarch, Thiqqums, CricKo, ClubPenguin,
606 RosaAsantewaa, and PherryCruz. Microbiol Resour Announc 11:e00922-22.

607 22. Arndt D, Grant JR, Marcu A, Sajed T, Pon A, Liang Y, Wishart DS. 2016. PHASTER: a better, faster
608 version of the PHAST phage search tool. Nucleic Acids Res 44:W16–W21.

609 23. Lorenzi J-N, Thibessard A, Lioy VS, Boccard F, Leblond P, Pernodet J-L, Bury-Moné S. 2022.
610 Ribosomal RNA operons define a central functional compartment in the *Streptomyces*
611 chromosome. Nucleic Acids Research 50:11654–11669.

612 24. Taylor VL, Fitzpatrick AD, Islam Z, Maxwell KL. 2019. The Diverse Impacts of Phage Morons on
613 Bacterial Fitness and Virulence, p. 1–31. *In* Advances in Virus Research. Elsevier.

614 25. Tong Y, Charusanti P, Zhang L, Weber T, Lee SY. 2015. CRISPR-Cas9 Based Engineering of
615 Actinomycetal Genomes. ACS Synth Biol 4:1020–9.

616 26. Lioy VS, Lorenzi J-N, Najah S, Poinsignon T, Leh H, Saulnier C, Aigle B, Lautru S, Thibessard A,
617 Lespinet O, Leblond P, Jaszczyszyn Y, Gorrichon K, Varoquaux N, Junier I, Boccard F, Pernodet J-L,
618 Bury-Moné S. 2021. Dynamics of the compartmentalized Streptomyces chromosome during
619 metabolic differentiation. Nat Commun 12:5221.

620 27. Haas D, Barba M, Vincente C, Nezbedova S, Garénaux A, Hôtel L, Thibessard A, Le Goff G, Ouazzani
621 J, Lautru S, Leblond P, Aigle B, Pernodet JL, Lespinet O. Synteruptor, a new comparative genomics-
622 based approach for identifying non-classical specialized metabolite gene clusters.

623 28. Thibessard A, Haas D, Gerbaud C, Aigle B, Lautru S, Pernodet JL, Leblond P. 2015. Complete
624 genome sequence of Streptomyces ambofaciens ATCC 23877, the spiramycin producer. J
625 Biotechnol 214:117–8.

626 29. Zimmermann L, Stephens A, Nam S-Z, Rau D, Kübler J, Lozajic M, Gabler F, Söding J, Lupas AN, Alva
627 V. 2018. A Completely Reimplemented MPI Bioinformatics Toolkit with a New HHpred Server at
628 its Core. Journal of Molecular Biology 430:2237–2243.

629 30. Terzian P, Olo Ndela E, Galiez C, Lossouarn J, Pérez Bucio RE, Mom R, Toussaint A, Petit M-A,
630 Enault F. 2021. PHROG: families of prokaryotic virus proteins clustered using remote homology.
631 NAR Genomics and Bioinformatics 3:lqab067.

632 31. Varet H, Brillet-Gueguen L, Coppee JY, Dillies MA. 2016. SARTools: A DESeq2- and EdgeR-Based R
633 Pipeline for Comprehensive Differential Analysis of RNA-Seq Data. PLoS One 11:e0157022.

634 32. R Core Team. 2022. R: A language and environment for statistical computing.

635 33. Scrucca L, Fop M, Murphy T Brendan, Raftery A E. 2016. mclust 5: Clustering, Classification and
636 Density Estimation Using Gaussian Finite Mixture Models. The R Journal 8:289.

637 34. Jakutytė L, Baptista C, São-José C, Daugelavičius R, Carballido-López R, Tavares P. 2011.
638 Bacteriophage Infection in Rod-Shaped Gram-Positive Bacteria: Evidence for a Preferential Polar
639 Route for Phage SPP1 Entry in Bacillus subtilis. J Bacteriol 193:4893–4903.

640 35. Misson P, Bruder E, Cornuault JK, De Paepe M, Nicolas P, Demarre G, Lakisic G, Petit M-A, Espeli O,
641 Lecointe F. 2023. Phage production is blocked in the adherent-invasive Escherichia coli LF82 upon
642 macrophage infection. PLoS Pathog 19:e1011127.

643 36. Djacem K, Tavares P, Oliveira L. 2017. Bacteriophage SPP1 pac Cleavage: A Precise Cut without
644 Sequence Specificity Requirement. Journal of Molecular Biology 429:1381–1395.

645 37. Robinson JT, Thorvaldsdottir H, Winckler W, Guttman M, Lander ES, Getz G, Mesirov JP. 2011.
646 Integrative genomics viewer. Nat Biotechnol 29:24–6.

647 38. Dobin A, Davis CA, Schlesinger F, Drenkow J, Zaleski C, Jha S, Batut P, Chaisson M, Gingeras TR.
648 2013. STAR: ultrafast universal RNA-seq aligner. Bioinformatics 29:15–21.

649 39. Liao Y, Smyth GK, Shi W. 2014. featureCounts: an efficient general purpose program for assigning
650 sequence reads to genomic features. Bioinformatics 30:923–30.

651 40. Garneau JR, Depardieu F, Fortier L-C, Bikard D, Monot M. 2017. PhageTerm: a tool for fast and
652 accurate determination of phage termini and packaging mechanism using next-generation
653 sequencing data. Sci Rep 7:8292.

654 41. Vingadassalon A, Lorieux F, Juguet M, Noël A, Santos LDF, Marin Fernandez L, Pernodet J-L, Bury-
655 Moné S, Lautru S. 2021. Transcriptional Regulation of Congocidine (Netropsin) Biosynthesis and
656 Resistance. Appl Environ Microbiol 87:e01380-21.

657 42. Bode HB, Bethe B, Hofs R, Zeeck A. 2002. Big effects from small changes: possible ways to explore
658 nature's chemical diversity. Chembiochem 3:619–27.

659 43. Hickey RJ, Tresner HD. 1952. A COBALT-CONTAINING MEDIUM FOR SPORULATION OF
660 STREPTOMYCES SPECIES. J Bacteriol 64:891–892.

661 44. Nagakubo T, Yamamoto T, Asamizu S, Toyofuku M, Nomura N, Onaka H. 2021. Phage tail-like
662 nanostructures affect microbial interactions between Streptomyces and fungi. Sci Rep 11:20116.

663 45. Vladimirov M, Zhang RX, Mak S, Nodwell JR, Davidson AR. 2023. A contractile injection system is
664 required for developmentally regulated cell death in Streptomyces coelicolor. Nat Commun
665 14:1469.

666 46. Tran NT, Huang X, Hong H, Bush MJ, Chandra G, Pinto D, Bibb MJ, Hutchings MI, Mascher T, Buttner
667 MJ. 2019. Defining the regulon of genes controlled by σ^E, a key regulator of the cell envelope
668 stress response in *Streptomyces coelicolor*. Mol Microbiol 112:461–481.

669 47. Tzanis A, Dalton KA, Hesketh A, Hengst CD, Buttner MJ, Thibessard A, Kelemen GH. 2014. A
670 sporulation-specific, *SIGF* -dependent protein, SSPA , affects septum positioning in *S treptomyces*
671 *coelicolor* . Molecular Microbiology 91:363–380.

672 48. Stratton KJ, Bush MJ, Chandra G, Stevenson CEM, Findlay KC, Schlimpert S. 2022. Genome-Wide
673 Identification of the LexA-Mediated DNA Damage Response in Streptomyces venezuelae. J
674 Bacteriol 204:e00108-22.

675 49. Feeney MA, Newitt JT, Addington E, Algora-Gallardo L, Allan C, Balis L, Birke AS, Castaño-Espriu L,
676 Charkoudian LK, Devine R, Gayrard D, Hamilton J, Hennrich O, Hoskisson PA, Keith-Baker M, Klein

677 JG, Kruasuwan W, Mark DR, Mast Y, McHugh RE, McLean TC, Mohit E, Munnoch JT, Murray J, Noble
678 K, Otani H, Parra J, Pereira CF, Perry L, Pintor-Escobar L, Pritchard L, Prudence SMM, Russell AH,
679 Schniete JK, Seipke RF, Sélem-Mojica N, Undabarrena A, Vind K, Van Wezel GP, Wilkinson B,
680 Worsley SF, Duncan KR, Fernández-Martínez LT, Hutchings MI. 2022. ActinoBase: tools and
681 protocols for researchers working on Streptomyces and other filamentous actinobacteria.
682 Microbial Genomics 8.

683 50. Becher PG, Verschut V, Bibb MJ, Bush MJ, Molnár BP, Barane E, Al-Bassam MM, Chandra G, Song L,
684 Challis GL, Buttner MJ, Flärdh K. 2020. Developmentally regulated volatiles geosmin and 2-
685 methylisoborneol attract a soil arthropod to Streptomyces bacteria promoting spore dispersal. Nat
686 Microbiol 5:821–829.

687 51. Hopwood DA. 2007. Streptomyces in nature and medicine: the antibiotic makers. Oxford
688 University Press, Oxford; New York.

689 52. Huang R, Lin J, Gao D, Zhang F, Yi L, Huang Y, Yan X, Duan Y, Zhu X. 2019. Discovery of gas vesicles
690 in Streptomyces sp. CB03234-S and potential effects of gas vesicle gene overexpression on
691 morphological and metabolic changes in streptomycetes. Appl Microbiol Biotechnol 103:5751–
692 5761.

693 53. Swiatek MA, Tenconi E, Rigali S, Van Wezel GP. 2012. Functional Analysis of the N-
694 Acetylglucosamine Metabolic Genes of Streptomyces coelicolor and Role in Control of
695 Development and Antibiotic Production. Journal of Bacteriology 194:1136–1144.

696 54. Jones SE, Ho L, Rees CA, Hill JE, Nodwell JR, Elliot MA. 2017. Streptomyces exploration is triggered
697 by fungal interactions and volatile signals. eLife 6:e21738.

698 55. Kieser T. BMJ Buttner MJ, Chater KF, Hopwood DA. 2000. Practical Streptomyces geneticsJohn
699 Innes Foundation, Norwich, United Kingdom.

700 56. van Wezel GP, Krabben P, Traag BA, Keijser BJF, Kerste R, Vijgenboom E, Heijnen JJ, Kraal B. 2006.
701 Unlocking *Streptomyces* spp. for Use as Sustainable Industrial Production Platforms by
702 Morphological Engineering. Appl Environ Microbiol 72:5283–5288.

703 57. Zacchetti B, Smits P, Claessen D. 2018. Dynamics of Pellet Fragmentation and Aggregation in
704 Liquid-Grown Cultures of Streptomyces lividans. Front Microbiol 9:943.

705 58. Manteca A, Rioseras B, González-Quiñónez N, Fernández-García G, Yagüe P. 2019. Mycelium
706 Differentiation and Development of *Streptomyces* in Liquid Nonsporulating Cultures: Programmed
707 Cell Death, Differentiation, and Lysis Condition Secondary Metabolite Production, p. . *In* Mishra, M
708 (ed.), Growing and Handling of Bacterial Cultures. IntechOpen.

709 59. Zhang Z, Shitut S, Claushuis B, Claessen D, Rozen DE. 2022. Mutational meltdown of putative
710 microbial altruists in Streptomyces coelicolor colonies. Nat Commun 13:2266.

711 60. Chang C, Yu X, Guo W, Guo C, Guo X, Li Q, Zhu Y. 2022. Bacteriophage-Mediated Control of Biofilm:
712 A Promising New Dawn for the Future. Front Microbiol 13:825828.

713 61. Rossmann FS, Racek T, Wobser D, Puchalka J, Rabener EM, Reiger M, Hendrickx APA, Diederich A-
714 K, Jung K, Klein C, Huebner J. 2015. Phage-mediated Dispersal of Biofilm and Distribution of
715 Bacterial Virulence Genes Is Induced by Quorum Sensing. PLoS Pathog 11:e1004653.

716 62. Rice SA, Tan CH, Mikkelsen PJ, Kung V, Woo J, Tay M, Hauser A, McDougald D, Webb JS, Kjelleberg
717 S. 2009. The biofilm life cycle and virulence of Pseudomonas aeruginosa are dependent on a
718 filamentous prophage. ISME J 3:271–282.

719 63. Black AJ, Bourrat P, Rainey PB. 2020. Ecological scaffolding and the evolution of individuality. Nat
720 Ecol Evol 4:426–436.

64. Smith MCM, Burns RN, Wilson SE, Gregory MA. 1999. The complete genome sequence of the Streptomyces temperate phage C31: evolutionary relationships to other viruses. Nucleic Acids Research 27:2145–2155.

65. Khaleel T, Younger E, McEwan AR, Varghese AS, Smith MCM. 2011. A phage protein that binds φC31 integrase to switch its directionality: Excision by φC31 integrase. Molecular Microbiology 80:1450–1463.

Figure Legends

Figure 1: Samy prophage identification by comparative genomics

A. Pairwise comparison of *S. ambofaciens* ATCC 23877 and DSM 40697 chromosomes. The grey line indicates the position of genes whose order is perfectly conserved between strains. The blue dots indicate areas of synteny break. The red circles correspond to genomic islands containing at least 20 CDS in one of the strains. The blue arrows indicate the position of xSAM1-pSAM2 integrated elements as well as the genomic island of interest harboring Samy prophage, detailed in the panels B and C. The central compartment (delimitated by the distal *rrn* operons) (26), the arms (defined as terminal regions devoid of core genes), the terminal inverted repeats (TIRs) and the position of the origin of replication (*oriC*) in *S. ambofaciens* ATCC 23877 chromosome are indicated. The level of gene order conservation between both strains as well as the GC percent content calculated in a window of 50 kb are indicated below the dot-blot.

B. Schematic representation of the genomic island containing the Samy prophage. The regions in which gene order is perfectly conserved in *S. ambofaciens* ATCC 23877 and DSM 40697 chromosomes are defined as the left and right synteny blocks (grey). The coordinates of the genomic island borders in *S. ambofaciens* ATCC 23877 strain are indicated in blue. The genomic island is composed of two regions: a remnant integrative element and the Samy prophage. These regions are separated by a short intergenic region (represented by an asterisk; 305 bp located from 6,589,473 to 6,589,777 bp) present in both strains. Two serine integrase coding sequences (red) have been predicted. The prophage also contains four tRNA encoding genes (pink).

C. Comparison of the Samy and PhiC31 phage genomes. Gene functions are color-coded as detailed in the legend. The annotation of PhiC31 genes was previously reported

in (64) and (65) (for the recombination directionality factor, RDF). Black vertical lines indicate the nine Samy genes identified as overexpressed compared to the entire Samy phage genome across all non or poorly-induced conditions (**Table S6**). The genome comparison was performed using Easyfig software (e-value $<10^{-3}$). The percentage identity between DNA homologous sequences in Samy and PhiC31 is shown in shades of gray. Other abbreviations: DNK (Deoxynucleoside monophosphate kinase), MCP (Major capsid protein), MTP (Major tail protein), TSS (Terminal small subunit), TLS (Terminal large subunit), TMP (Tape measure protein).

Figure 2: Massive awakening of mobile genetic elements in HT medium

A. Heatmap of Samy region transcription in different growth conditions. Normalized RNA-seq data (**Table S5**) were categorized in a color scale reflecting the expression of each gene relative to whole genome expression in each condition, as indicated in the Annotation legend. Each line represents a gene, ranked according to their order on the genome. For the remnant integrative element as well as for Samy prophage, a prediction of the gene product is indicated when available. Growth conditions (columns) are ranked by hierarchical clustering according to Samy transcriptome profiles. The growth conditions are detailed in **Fig. S3.A** and **Table S3**. Phage genes of predicted function that stand out as overexpressed compared to the entire Samy phage genome across at least six non or poorly-induced conditions (**Table S6**) are written in bold.

B. Plot of the log ratio of differential expression as a function of gene expression after 30 h growth in HT solid medium compared to 24 h growth in liquid MP5 medium. The color of differentially expressed genes (adjusted p value < 0.05) is indicated. The number of regulated genes relative to the total number of genes is shown in parentheses for the mobile genetic elements of interest.

Figure 3: Impact of medium composition on Samy phage production, final pH and antibacterial activity of *S. ambofaciens* ATCC 23877 supernatants

The supernatants of *S. ambofaciens* ATCC 23877 grown in different media (composition summarized below the graph and detailed in **Table S3**) were harvested after 4 days and 0.2 µm-filtered. Phage titer was determined by qPCR after DNAse treatment. The pH of the medium and the antibacterial activity against *Micrococcus luteus* of the supernatant after 4 days of growth are indicated on the top. All media had an initial pH of 7.3 (± 0.1), except MP5 and MP5 devoid of MOPS which had a pH of 7.5 (± 0.1). All the

boxplots represent the first quartile, median and third quartile. The upper whisker extends from the hinge to the largest value no further than 1.5 * the inter-quartile range (IQR, *i.e*. distance between the first and third quartiles). The lower whisker extends from the hinge to the smallest value at most 1.5 * IQR of the hinge. Each dot represents an independent experiment. The *p* values of two-sided Wilcoxon rank sum tests with continuity correction is indicated for each comparison to the viral titer observed in HT condition.

Figure 4: Samy phage production and morphology

A. Kinetics of phage production. *S. ambofaciens* ATCC 23877 was grown in BM medium. The viral titer of supernatants filtered and DNAse-treated were determined by qPCR. Each color represents an independent experiment. The boxplot is plotted as described in the legend of **Fig. 3**. The *p* value of two-sided Wilcoxon rank sum tests with continuity correction is 0.0294 when comparing the viral titers at 24 h and 48h, and 1 (no difference) when comparing the evolution of the titer on the following days.

B. Imaging of Samy phage produced by transmission electron microscopy. *S. ambofaciens* ATCC 23877 was grown during 4 days in BM medium. The supernatant was concentrated by CsCl-gradient ultracentrifugation. Viral particles were negatively stained with uranyl acetate (also see **Figure S6.A & B**). Scale bar: 100 nm.

Figure 5: Dispersion phenotype associated with the production of the Samy phage

A. Growth and pH in BM and MP5 media. Each symbol represents an independent experiment. Due to the presence of large aggregates (see panel B), the pseudo-opacimetry ($OD_{600\ nm}$) was not exploitable for DSM 40697 strain after 48h of growth in BM medium.

B. Dispersed *versus* aggregated growth of *S. ambofaciens* strains in BM media. The results are representative of the appearance of the most frequently observed cultures, as the quantity and size of cell clusters may vary from one experiment to the other. The *S. ambofaciens* ATCC 23877 Δ*Samy* strain corresponds to clone #3, deleted from at least the phage integrase by a CRIPSR-based approach (**Table S1, Figure S1**). Scale bar: 1.5 cm.

C. Microscopy of *Streptomyces* colonies after 4 days growth in BM medium. *S. ambofaciens* ATCC 23877 and its derivate CRISPR-deleted of Samy prophage (clone #3) were grown in BM medium and imaged using differential interference contrast microscopy (also see **Figure S8.A**). Scale bar: 10 µm.

D. Colony forming units after 4 days of growth in BM medium. The *S. ambofaciens* ATCC 23877 ΔSamy strains correspond to three independent mutants (#1, #3 and #4) we

obtained by a CRIPSR-based approach (**Table S1**). The boxplot is plotted as described in the legend of **Fig. 3**. Each dot represents an independent experiment per condition. The *p* values of two-sided Wilcoxon rank sum tests with continuity correction are indicated for each comparison. Please note that this number is the result of both cell survival and mycelium dispersal (propensity to form separate colonies).

E. Correlation between Samy phage production and colony forming units by diverse *S. ambofaciens* strains. *S. ambofaciens* strains obtained from distinct collections (**Table S1**) were grown during 4 days in BM medium, before counting colony forming units and phage production in the supernatants. Even strains ATCC 23877 and DSM 40697 were cultured for this experiment from stocks produced by another laboratory. Each dot represents an independent experiment per strain. The correlation was analyzed by a Spearman's rank correlation test. Results of two independent experiments.

F. **Bioassay performed with the supernatants of *S. ambofaciens* ATCC 23877 WT strain and its derivatives deleted in Samy regions** (clones #1, #3 and #4 - **Table S1, Figure S1**). Fifty microliters of filtered supernatant from *S. ambofaciens* culture after 4 days in BM medium was deposited on a *Micrococcus luteus* mat, as previously described (26). The size of the *M. luteus* growth inhibition halo after 24 h incubation at 37°C was measured. The boxplot is plotted as described in the legend of **Fig. 3**. The *p* values of two-sided Wilcoxon rank sum tests with continuity correction are indicated.

Figure 6: Model of the stress- and phage-induced dispersed growth of *Streptomyces* in liquid medium

After germination of the spore, the multicellular bacteria form successively primary and secondary mycelia. In the absence of prophage, the *S. ambofaciens* DSM 40497 tends to form particularly large and dense pellets in response to metabolic stress encountered in BM medium (nitrogen unbalance, translation inhibition, basic pH). Under the same conditions, phage production by *S. ambofaciens* ATCC 23877 is correlated with dispersed growth in sparse clumps and filaments. We propose that phage-induced cell death within the secondary mycelium leads to a dislocation of multicellular aggregates. The subsequent increase in the number of small colonies promotes strain dispersal under stressful conditions.

Figure 1

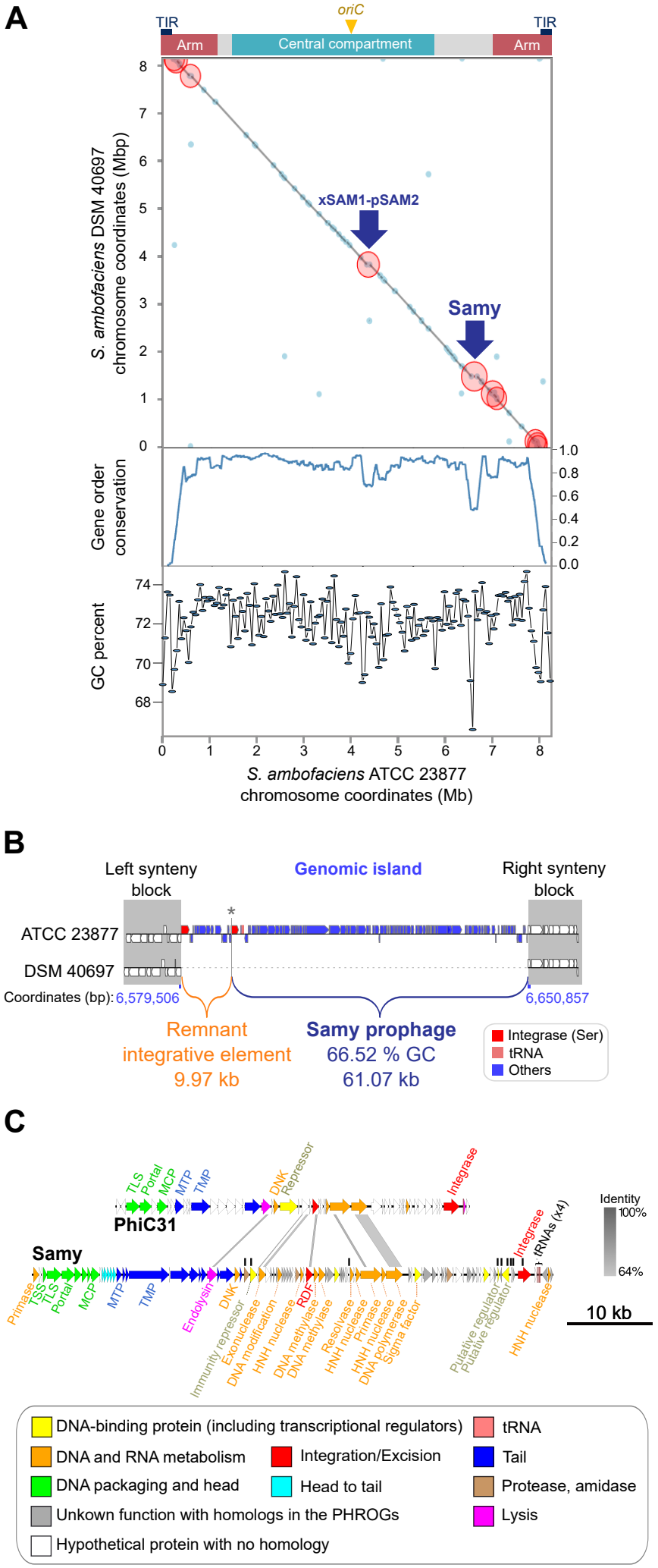
A
TIR
oriC
TIR
Arm
Central compartment
Arm
S. ambofaciens DSM 40697 chromosome coordinates (Mbp)
xSAM1-pSAM2
Samy
Gene order conservation
GC percent
S. ambofaciens ATCC 23877 chromosome coordinates (Mb)
B
Left synteny block
Genomic island
Right synteny block
ATCC 23877
DSM 40697
Coordinates (bp): 6,579,506
6,650,857
Remnant integrative element 9.97 kb
Samy prophage 66.52 % GC 61.07 kb
Integrase (Ser)
tRNA
Others
C
PhiC31
Samy
Integrase
tRNAs (x4)
Identity
100%
64%
10 kb
DNA-binding protein (including transcriptional regulators)
DNA and RNA metabolism
DNA packaging and head
Unkown function with homologs in the PHROGs
Hypothetical protein with no homology
Integration/Excision
Head to tail
tRNA
Tail
Protease, amidase
Lysis

Figure 2

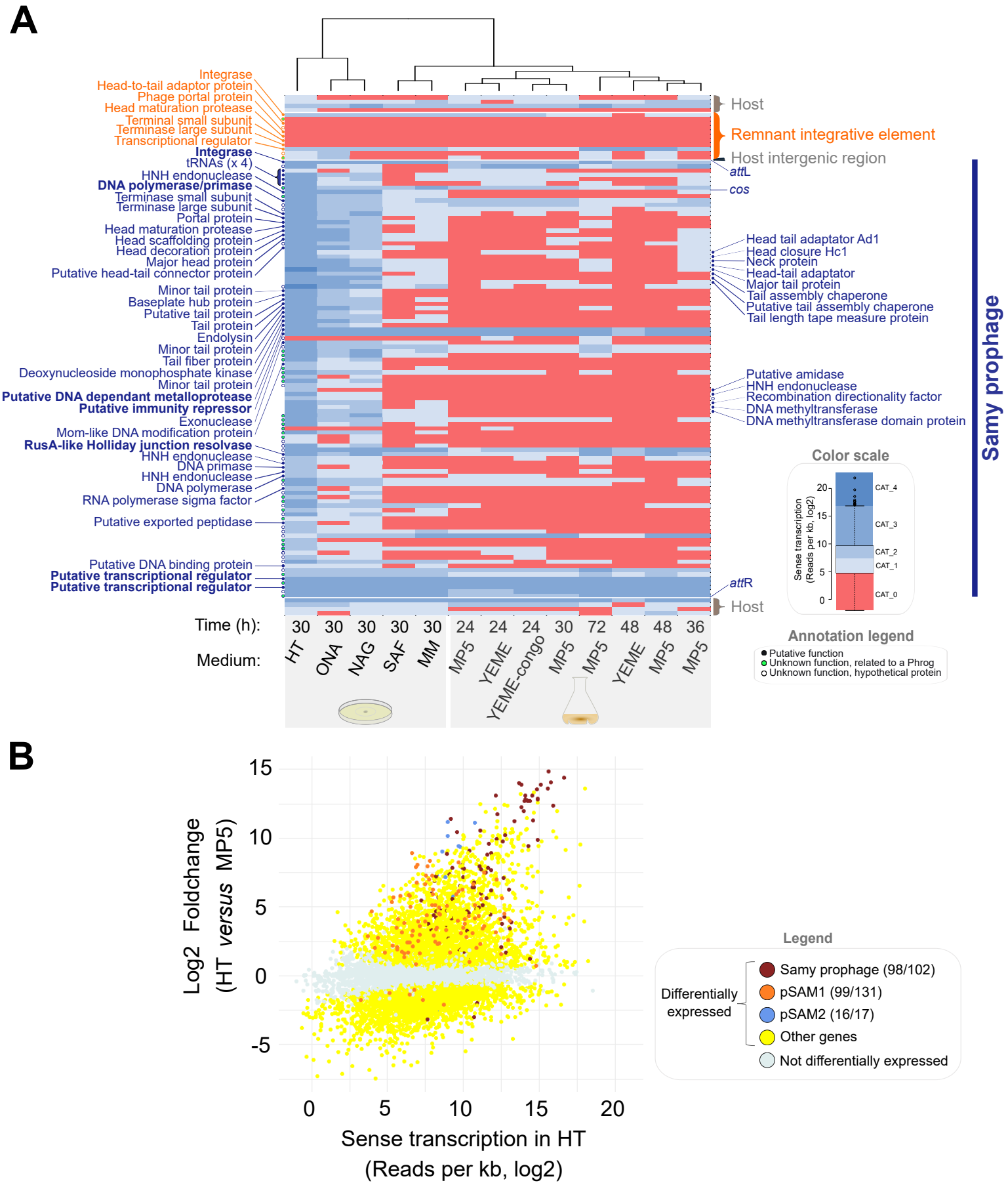
A
Integrase
Head-to-tail adaptor protein
Phage portal protein
Head maturation protease
Terminal small subunit
Terminase large subunit
Transcriptional regulator
Integrase
tRNAs (x 4)
HNH endonuclease
DNA polymerase/primase
Terminase small subunit
Terminase large subunit
Portal protein
Head maturation protease
Head scaffolding protein
Head decoration protein
Major head protein
Putative head-tail connector protein
Minor tail protein
Baseplate hub protein
Putative tail protein
Tail protein
Endolysin
Minor tail protein
Tail fiber protein
Deoxynucleoside monophosphate kinase
Minor tail protein
Putative DNA dependant metalloprotease
Putative immunity repressor
Exonuclease
Mom-like DNA modification protein
RusA-like Holliday junction resolvase
HNH endonuclease
DNA primase
HNH endonuclease
DNA polymerase
RNA polymerase sigma factor
Putative exported peptidase
Putative DNA binding protein
Putative transcriptional regulator
Putative transcriptional regulator
Host
Remnant integrative element
Host intergenic region
attL
cos
Head tail adaptator Ad1
Head closure Hc1
Neck protein
Head-tail adaptator
Major tail protein
Tail assembly chaperone
Putative tail assembly chaperone
Tail length tape measure protein
Putative amidase
HNH endonuclease
Recombination directionality factor
DNA methyltransferase
DNA methyltransferase domain protein
attR
Host
Samy prophage
Time (h):
30 30 30 30 30 24 24 24 30 72 48 48 36
Medium:
HT ONA NAG SAF MM MP5 YEME YEME-congo MP5 MP5 YEME MP5 MP5
Color scale
Sense transcription (Reads per kb, log2)
CAT_4
CAT_3
CAT_2
CAT_1
CAT_0
Annotation legend
Putative function
Unknown function, related to a Phrog
Unknown function, hypothetical protein
B
Log2 Foldchange (HT versus MP5)
Sense transcription in HT (Reads per kb, log2)
Legend
Differentially expressed
Samy prophage (98/102)
pSAM1 (99/131)
pSAM2 (16/17)
Other genes
Not differentially expressed

Figure 3

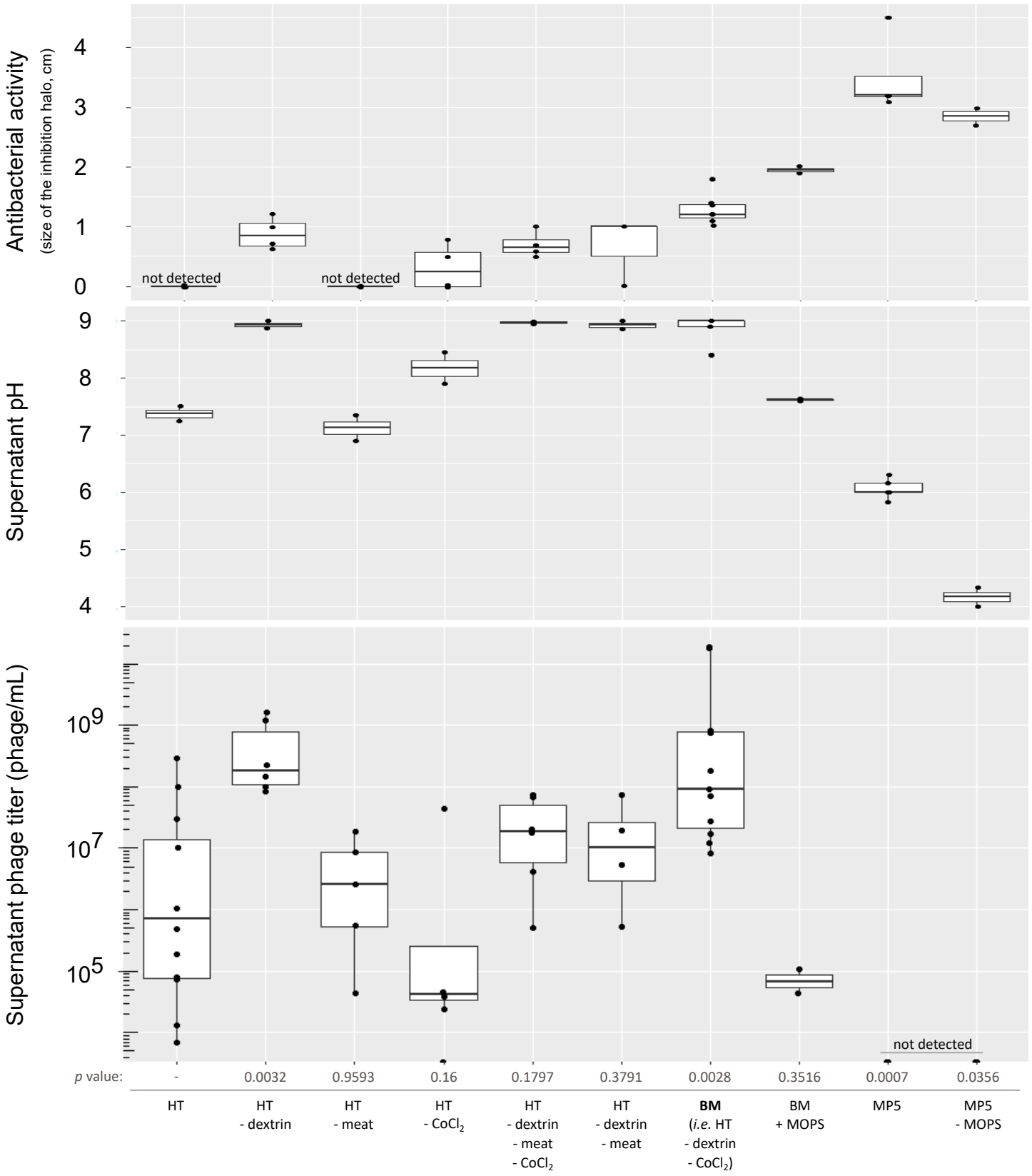
Antibacterial activity
(size of the inhibition halo, cm)
4
3
2
1
0
not detected
not detected
Supernatant pH
9
8
7
6
5
4
Supernatant phage titer (phage/mL)
10^9
10^7
10^5
not detected
p value:
-
0.0032
0.9593
0.16
0.1797
0.3791
0.0028
0.3516
0.0007
0.0356
HT
HT - dextrin
HT - meat
HT - $CoCl_2$
HT - dextrin - meat - $CoCl_2$
HT - dextrin - meat
BM (*i.e.* HT - dextrin - $CoCl_2$)
BM + MOPS
MP5
MP5 - MOPS

Figure 4

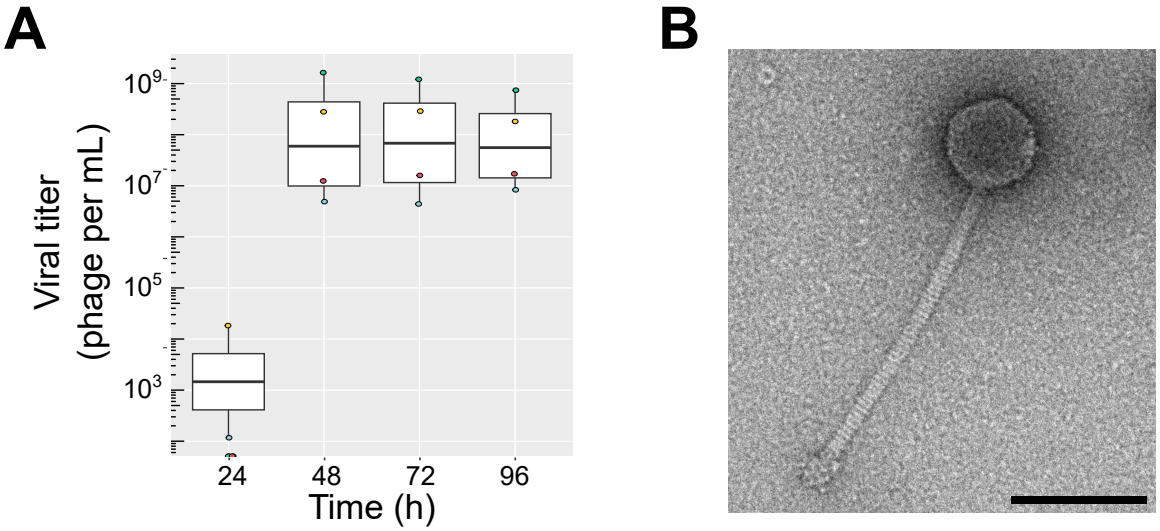

Figure 5

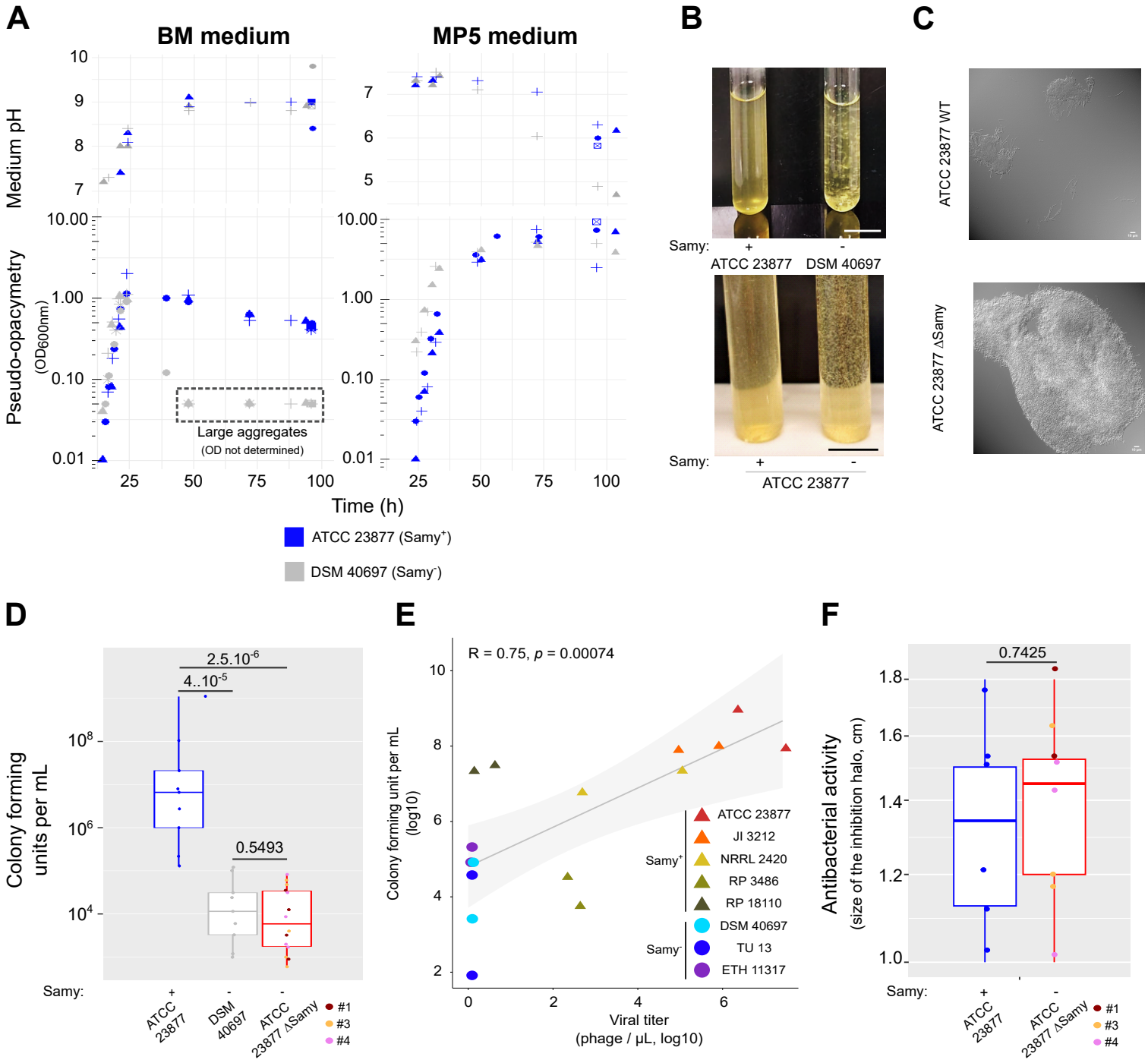
A
BM medium
MP5 medium
Medium pH
Pseudo-opacymetry
(OD600nm)
Large aggregates
(OD not determined)
Time (h)
ATCC 23877 (Samy+)
DSM 40697 (Samy-)
B
Samy:
+
-
ATCC 23877
DSM 40697
C
ATCC 23877 WT
ATCC 23877 ΔSamy
D
Colony forming units per mL
2.5.10-6
4..10-5
0.5493
Samy:
ATCC 23877
DSM 40697
ATCC 23877 ΔSamy
#1
#3
#4
E
R = 0.75, p = 0.00074
Colony forming unit per mL (log10)
Viral titer (phage / µL, log10)
Samy+
Samy-
ATCC 23877
JI 3212
NRRL 2420
RP 3486
RP 18110
DSM 40697
TU 13
ETH 11317
F
0.7425
Antibacterial activity
(size of the inhibition halo, cm)
Samy:
ATCC 23877
ATCC 23877 ΔSamy
#1
#3
#4

Figure 6

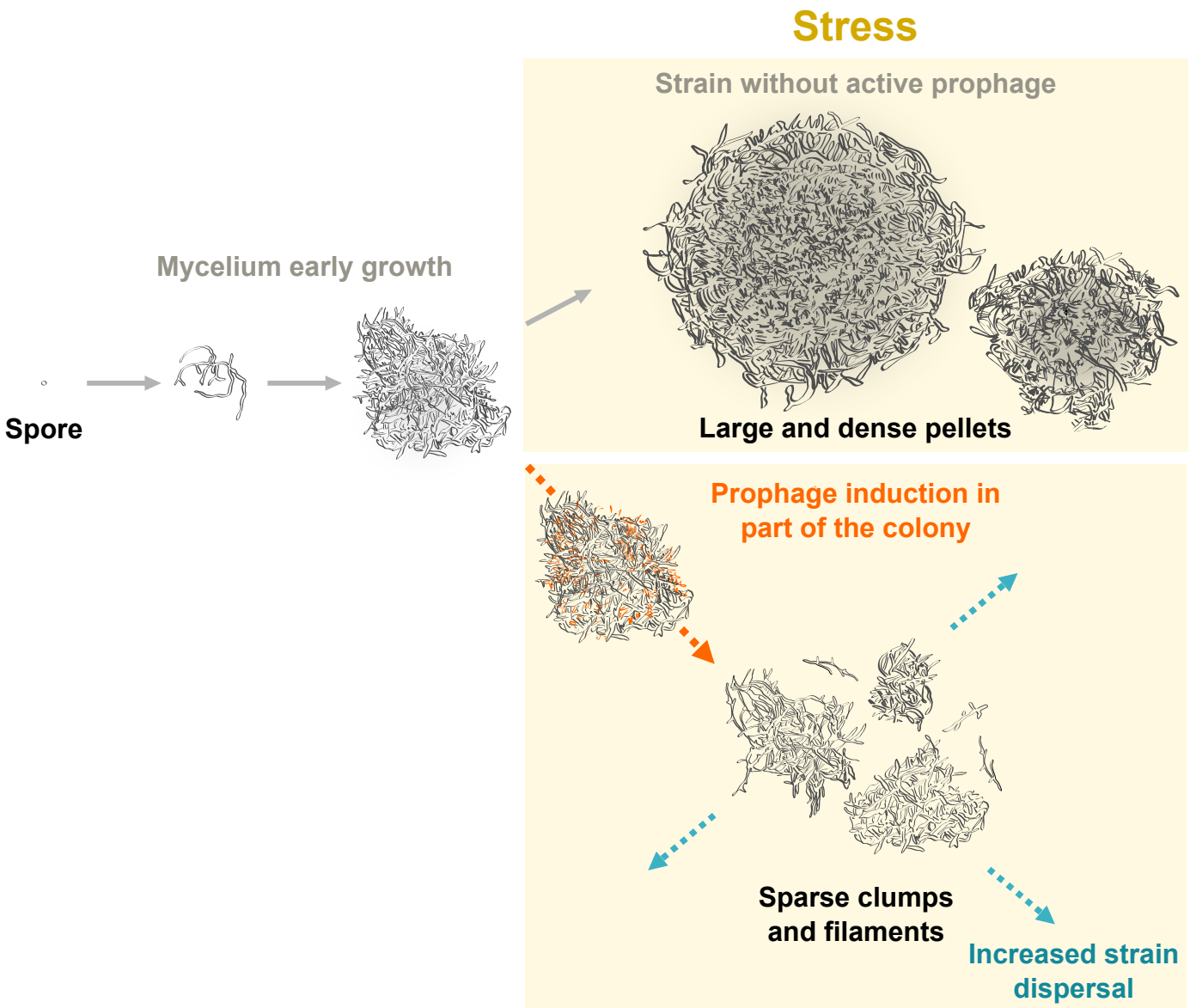
Stress
Strain without active prophage
Mycelium early growth
Spore
Large and dense pellets
Prophage induction in part of the colony
Sparse clumps and filaments
Increased strain dispersal
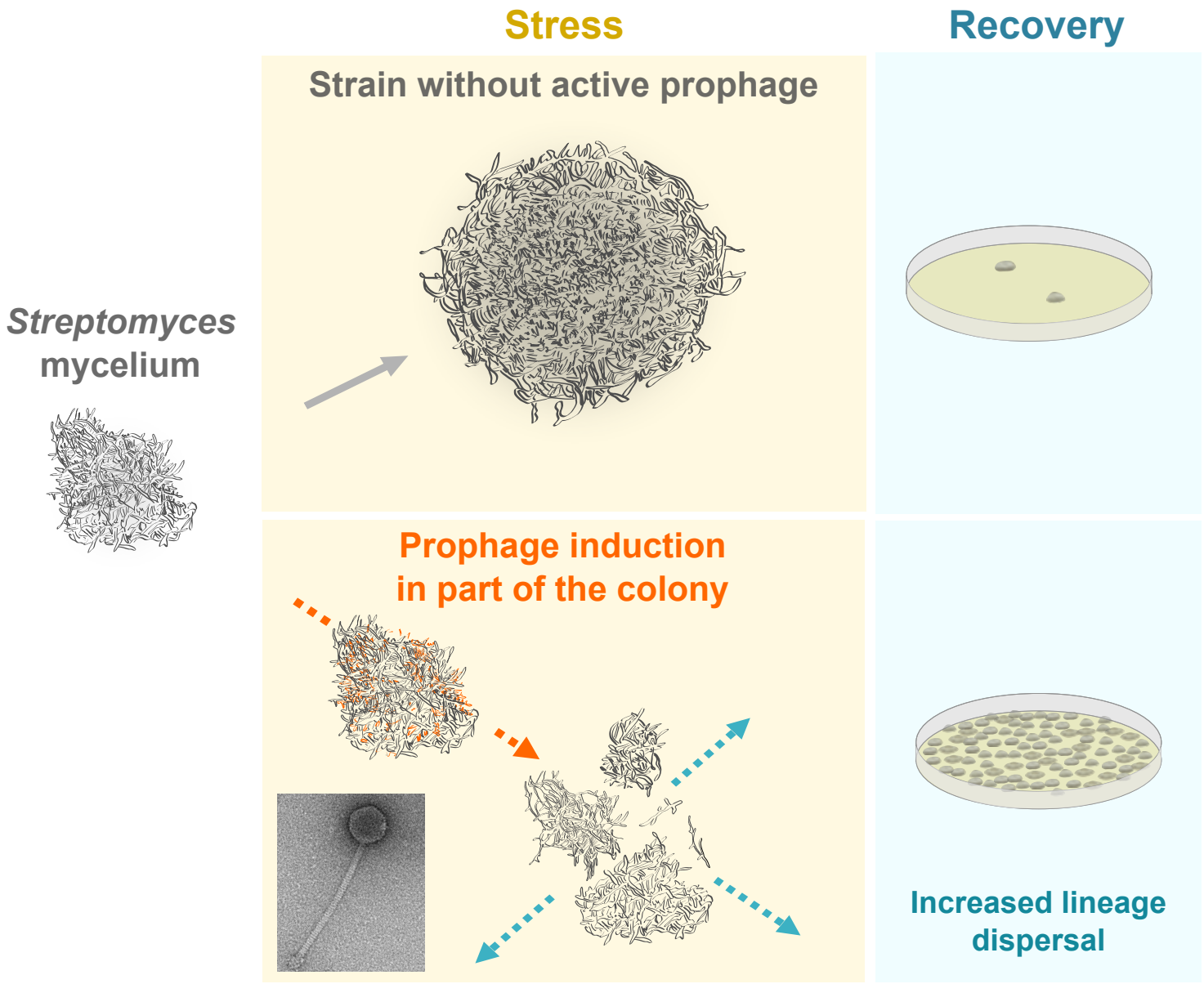
Graphical summary